Favorable Concurrence of Static and Dynamic Phenomena at the Morphotropic Phase Boundary of xBiNi_{0.5}Zr_{0.5}O_{3}-(1-x)PbTiO_{3}

K. Datta, R. B. Neder, J. Chen, J. C. Neuefeind, and B. Mihailova

Phys. Rev. Lett. **119**, 207604 — Published 16 November 2017

DOI: 10.1103/PhysRevLett.119.207604

Favorable concurrence of static and dynamic phenomena at the morphotropic phase boundary of xBiNi$_{0.5}$Zr$_{0.5}$O$_3$-(1-x)PbTiO$_3$

K. Datta,[1] R. B. Neder,[2] J. Chen,[3] J. C. Neuefeind,[4] and B. Mihailova[1]

[1] *Department of Earth Sciences, University of Hamburg, Hamburg 20146, Germany.*[*]
[2] *Department of Crystallography and Structure Physics, Friedrich-Alexander-Universität Erlangen-Nürnberg, Staudtstrasse 3, Erlangen 91058, Germany.*
[3] *School of Metallurgical and Ecological Engineering, University of Science and Technology Beijing, Beijing 100083, China.*
[4] *Chemical and Engineering Materials Division, Oak Ridge National Laboratory, Oak Ridge, Tennessee 37831, United States.*

We reveal that concurrent events of inherent entropy-boosting and increased synchronization between A- and B-site cations vibrations of a ABO_3-type perovskite structure give rise to larger piezoelectric response in a ferroelectric system at its morphotropic phase boundary (MPB). It is further evident that the superior piezoelectric properties of xBiNi$_{0.5}$Zr$_{0.5}$O$_3$-(1-x)PbTiO$_3$ in comparison to xBiNi$_{0.5}$Ti$_{0.5}$O$_3$-(1-x)PbTiO$_3$ is due to the absolute flattening of the local potentials for all ferroelectrically active cations with higher spontaneous polarization at the MPB. These distinctive features have been discovered from the analyses of neutron pair distribution functions and Raman scattering data at ambient conditions, which are particularly sensitive to mesoscopic-scale structural correlations. Altogether this uncovers more fundamental structure-property connections for ferroelectric systems exhibiting MPB, and thereby has critical impact in contriving efficient novel materials.

Perovskite-based ferroelectric materials are an important class of functional materials and a key topic in materials science. One of the major challenges in this field is to build rigorous and generic structure-property relationships to better understand the morphotropic phase boundary (MPB) where physical properties are enhanced anomalously. The manifestation of superior properties on the onset of an MPB has been broadly discussed so far in the light of structure and thermodynamics as the existence of low-symmetry phases and the overall flattening of the free energy surfaces or structural instabilities, respetively, which facilitate the polarization-rotation under external stimuli.[1–5] However these prevailing concepts cannot fully identify the distinctive system-dependent atomistic mechanism in order to explain the comparative behavior – a key ingredient for developing efficient and benign materials. The complexity of this problem arises from the existence of multiple competing structural correlations, such as chemical order, correlated displacement, octahedral tilts and different types of bonding in a multi-component ferroic system, which are often very subtle to be categorized distinctly in a quantitative or qualitative manner.[6–8] Although there have been many recent experimental attempts to build more convincing structural models mimicking the atomic-level structural correlations in complex systems,[9–17] the challenge in formulating robust atomistic model still exists.

In this context, we have applied total neutron scattering and Ramam scattering methods to two promising ferroeletric solid solutions xBiNi$_{0.5}$Ti$_{0.5}$O$_3$-(1-x)PbTiO$_3$ (xBNT-PT) and xBiNi$_{0.5}$Zr$_{0.5}$O$_3$-(1-x)PbTiO$_3$ (xBNZ-PT), in order to establish structure-property connections based on atomic-level information.

Perovskite-based ferroelectric systems with the general formula xBiMeO$_3$-(1-x)PbTiO$_3$ became hugely popular lately because of their excellent physical properties with broader range of operating temperatures, and moreover due to their reduced Pb-content in comparison to PbZr$_x$Ti$_{1-x}$O$_3$, which has been the material of choice for the last four decades. In particular, xBNZ-PT has attracted a lot of attention because of its unusually high piezoelectric coefficients at $x_{\mathrm{MPB}} = 0.40$ relative to its parent system xBNT-PT ($d_{33} \sim 400$ pC/N and 260 pC/N, respectively).[18,19] It has further advantage of being inexpensive because of the raw materials compared to BiScO$_3$-PbTiO$_3$[20] and BiNi$_{0.5}$Hf$_{0.5}$O$_3$-PbTiO$_3$.[21] Therefore it is considered as a promising candidate to replace the currently used piezoelectric materials.[22]

In this letter, we focus on the key question: why does xBNZ-PT demonstrate better piezoelectric properties than the xBNT-PT at MPB? In doing so, we reveal how the incorporation of Zr^{4+} at the B-sublattice influences the structural disorder at the mesoscopic scale and subsequently, combined with the cooperative A- and B-site atomic vibrations, generates favorable conditions for better piezoelectric properties. The discovered local structural features in general provide a new approach to develop more inclusive structure-property relations in ferroelectric solid solutions with MPBs.

Room temperature neutron powder diffraction experiments on xBNT-PT and xBNZ-PT ceramics – produced by typical solid state synthesis method[18,23] – were carried out at the NOMAD beamline in Oak Ridge national laboratory (ORNL). Pair distribution functions (PDF) were obtained through running a data-correction procedure followed by the Fourier transformations with a maximum reciprocal-space vector Q of 31.4 Å^{-1}. The modelings of the PDFs were done using the RMCprofile package, which performs typical big-box modeling implementing the reverse Monte Carlo (RMC) technique.[24,25] Analyses of the RMC-refined structural models were done using the various tools available as part of the DIS-

CUS software.[26] Complementary room-temperature Raman scattering data as a function of composition were collected with a Horiba Jobin-Ivon T64000 spectrometer with spectral resolution of 2 cm^{-1} and peak-position precision of 0.35 cm^{-1}. More details on experiments and analyses are given in the supplemental material (SM)[27].

Given the fact that most of the technological interests in ferroelectric materials including their piezoelectric and dielectric properties are governed by their spontaneous polarization, we have examined the inherent polar displacements $\delta\vec{r}$ of the cations calculated with respect to the center of their corresponding oxygen environment, as schematically shown in Fig.1.[6,15,16,28] The distributions of the magnitudes $|\delta\vec{r}|$ and the directions $\delta\hat{r}$ of the displacements were extracted from the RMC-refined structural models. Figure 2 shows the development of such direction-distributions as a function of composition for both xBNT-PT and xBNZ-PT, where directions are mapped onto the standard $[001]_{pc}$ (pc refers to pseudocubic setting) stereograph. Primarily, the maps depict the evolution of the statistical trend of $\delta\hat{r}$ with composition reflecting the long-range or the Bragg symmetry of the system. However beyond that, the maps virtually describes the local correlations of the polar displacements in terms of their ordering, or in other words the variations of the local polarization directions within the system in its virgin state. Hence one can also relate these graphs to the atomic-scale order-disorder characteristics, from which it is possible to envisage the development of the local potential surfaces of each cation with x.

In order to quantify the observed statistical information of $\delta\hat{r}$, we have calculated the so-called orientational order paramerter $S = 1.5\langle\cos^2\theta\rangle - 0.5$ (see Fig.3), where θ is the angle between $[001]_{pc}$ and $\delta\vec{r}$. The parameter S simply signifies the extent of randomness in directions when the distributions are more or less symmetric around the chosen director, which is $[001]_{pc}$ here. Therefore it is evident that as x increases, both systems exhibit gradual increase in disorder characterized by the stochasticity of intrinsic polar order. Notably, xBNZ-PT differs from xBNT-PT by the fact that both A- and B-site cations have similar level of randomness (comparable S values), while in xBNT-PT, B-site cations show higher level of disorder (lower S values) than A-site cations in the range $0.20 \leq x \leq x_{\mathrm{MPB}}$. This indicates that the isovalent substitution of Zr^{4+} significantly affects the ferroic order of the A-site cations – presumably through enhanced local elastic stress caused by the larger ionic radius of Zr^{4+}, which subsequently shifts the MPB at a lower value of x compared to that of xBNT-PT.

It is interesting to see that, the MPB of xBNT-PT and xBNZ-PT at $x = 0.55$ and 0.40, respectively, can be straightway told apart from the development of the $\{002\}_{pc}$ Bragg peak (Fig. 2a), but the short-range neutron PDFs (Fig. S2) exhibit gradual change with increasing x. Therefore together with the stereographs, it provides direct evidence that the composition-directed phase transformations are more of a order-disorder type than a displacive type, which is generally considered as a signature feature of ferroelectric solid solutions with MPBs. In addition, we have not detected any chemical ordering at A- or B-site cation sublattices in our refined models for both cases(Fig. S6), defying some reported assumptions based on the theoretical calculations on analogous systems.[30,31] The stereographs of xBNT-PT also point out that A-site cations maintain a strong $[001]_{pc}$-type directional preference at MPB, while in xBNZ-PT both A- and B-site cations simultaneously exhibit pronounced dispersion of $\delta\hat{r}$ at $x = x_{\mathrm{MPB}}$. The prominent $[001]_{pc}$ propensity of A-site cation displacements in xBNT-PT in fact nicely complements the recent study which detected substantial inherent tetragonal domain alignment before poling.[32]

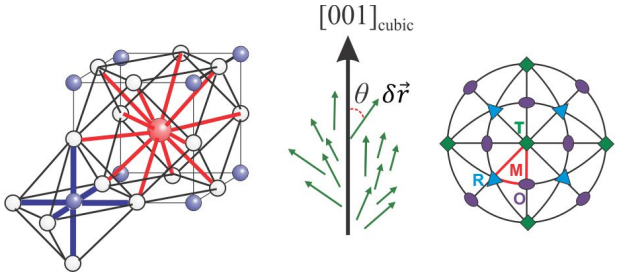

FIG. 1. Schematics of an aristotype perovskite structure showing the 12 and 6 oxygen neighbors of A- (red) and B-site (blue) cation, respectively. On the right a typical $[001]_{cubic}$ stereograph onto which the directions of the polar displacements ($\delta\vec{r}$) have been mapped.

Figure 4 demonstrates the variations of $|\delta\vec{r}|_{\mathrm{mean}}$ along with their standard deviations ($\sigma(|\delta\vec{r}|)$) as a function of x, which were estimated from the histograms of the magnitudes of the polar shifts (Fig. S7). It is evident that the addition of larger Zr^{4+} ($r_{\mathrm{ionic}} = 0.78$ Å) induces greater shifts for the A-site cations as well as larger standard deviations (Fig.4c and d). Importantly though, in both systems the A-site cation displacements remain relatively constant with x (average $|\delta\vec{r}|_{\mathrm{mean}} = 0.40$ and 0.45 Å for xBNT-PT and xBNZ-PT, respectively), whereas the B-site cations in xBNZ-PT show a decrease in $|\delta\vec{r}|_{\mathrm{mean}}$ upon approaching to the MPB from $x = 0.20$, justifying the fact that Pb-based ferroelectrics are predominantly A-site driven ferroelectrics.[33,34]

So far it appears that the superior piezoelectric properties of xBNZ-PT at MPB is stemming from the higher structural disorder characterized by local random ferroelectric order together with the increased A-site cation shifts with respect to that of xBNT-PT. However this cannot explain the drop in the piezoelectric coefficient just above or below the exact MPB composition in both systems (Fig.5). For instance, xBNT-PT does not render better piezoelectric properties at $x = 0.60$ where the cations exhibit very similar values of $|\delta\vec{r}|_{\mathrm{mean}}$ including the highest orientational disorder of the shifts. Therefore, considering the above facts one can draw out a few inferences: the gross enhancement phenomenon for a par-

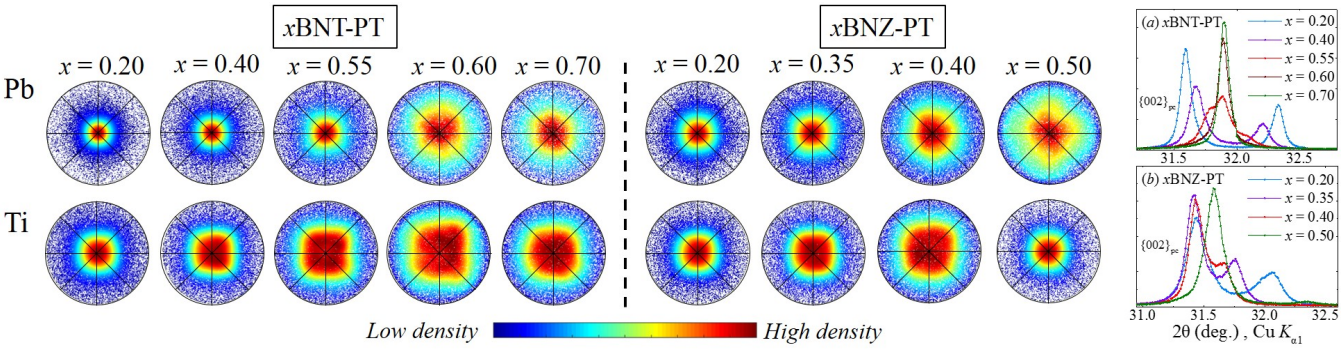

FIG. 2. Stereographs of the directions ($\widehat{\delta r}$) of polar displacements as obtained from the refined structural models as a function of composition. The colors exhibit the density distribution around each point on the graph and therefore help to classify the statistical trend in terms of their symmetry. On the right, the development of $\{002\}_{pc}$ Bragg reflection for both compounds obtained from the laboratory x-ray diffraction experiments. The stereographs of the other A- and B-site cations as a function of composition are included in SM (Fig. S4)

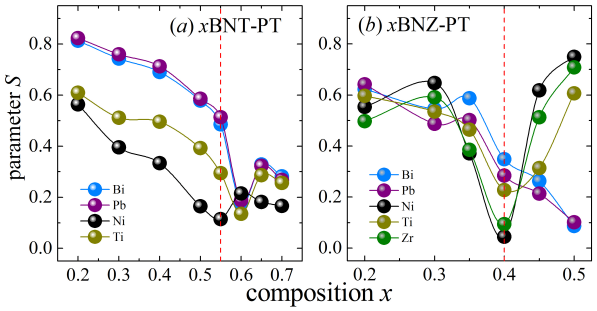

FIG. 3. Development of parameter S for A- and B- site cations as a function composition for both solid solutions.

ticular system is thoroughly driven by the so-called extrinsic contributors as the combined variation of $|\delta\vec{r}|$ cannot account for the observed enhancement at $x = x_{\mathrm{MPB}}$. Secondly, the exact or the relative values of piezoelectric properties cannot be fully anticipated considering solely the concepts based on ferroelectric instabilities. It may well be a necessary factor but surely not sufficient in order to deliver the amplification at the MPBs, because equilibrium atomic configurations with different composition exhibiting similar disorder differ significantly in their properties (Fig.5).

The quest for a more comprehensive answer to the above puzzle lead us to investigate the room-temperature Raman scattering data in order to gather complementary information related to atomic dynamics. The deconvolution of the Raman spectra through rigorous peak-fitting procedure helps to follow the development of distinctive A- and B-site cation vibrations as a function of composition. The respective peaks were categorized following the previously reported assignments.[17,35–37] Figure 6 shows the development of two deduced factors typically considered for a two-component behavior : (1) average of squared wavenumbers $< \omega >= \sqrt{\frac{\omega_i^2+\omega_j^2}{2}}$ and (2) normalized difference $\Delta\omega = \frac{\omega_i^2-\omega_j^2}{2(\omega_i^2+\omega_j^2)}$, which reveal specific similarities and differences in the overall characteristics of the two systems. The $< \omega >$ reflects the average dynamic energy state of a given type of atoms, while $\Delta\omega$ represents the energy difference between the distinct dynamic states and thereby describes the local structural anisotropy. Evidently, the $< \omega_{\mathrm{A}} >$ involving mainly A-site cation vibrations (ω_1 and ω_2 in Fig. S9) demonstrate a prominent softening at MPB (Fig.6a). However, the softening in the case of xBNZ-PT is much stronger than that in xBNT-PT. The development of $\Delta\omega$ illustrates another important difference in the thermodynamic picture between the two systems: A-site cations in xBNZ-PT experience complete flattening ($\Delta\omega_{\mathrm{A}} = 0$) in their local potential at MPB, whereas in xBNT-PT there are still distinguishable energy states with diminished energy barriers as $\Delta\omega_{\mathrm{A}}$ remains non-zero throughout the composition-range (Fig.6a inset).

On the other hand, the B-site cations exhibit gradual hardening of $< \omega >_{\mathrm{B}}$ in xBNT-PT with increasing x (inset of Fig.6c), whereas $< \omega >_{\mathrm{B}}$ softens at MPB for xBNZ-PT. Nevertheless, the two components of the B-site cations eventually merge into a single peak at MPB in both cases ($\Delta\omega_{\mathrm{B}} = 0$ in Fig.6c) and reveal the concomitant flattening of the corresponding local potential surfaces.

Nevertheless, the most interesting feature from the Raman scattering data can be pointed out from Fig.6b, which displays the softening of the A-BO_3 phonon mode (ω_3) at the MPBs of both systems. This mode comprises the vibrations of both A- and B-site cations corresponding to a T_{1u} phonon in the aristotype $Pm\bar{3}m$ structure.[35] Such a softening as a distinctive phenomenon has been also detected in xBiMg$_{0.5}$Ti$_{0.5}$O$_3$-(1-x)PbTiO$_3$[17] and (1-x)Na$_{0.5}$Bi$_{0.5}$TiO$_3$-xBaTiO$_3$[36]. Hence the ubiquitousness of this increased dynamic coupling between A- and B-site cations occurring precisely at the MPBs provides a new perspective based on the dynamics of the atomic vibra-

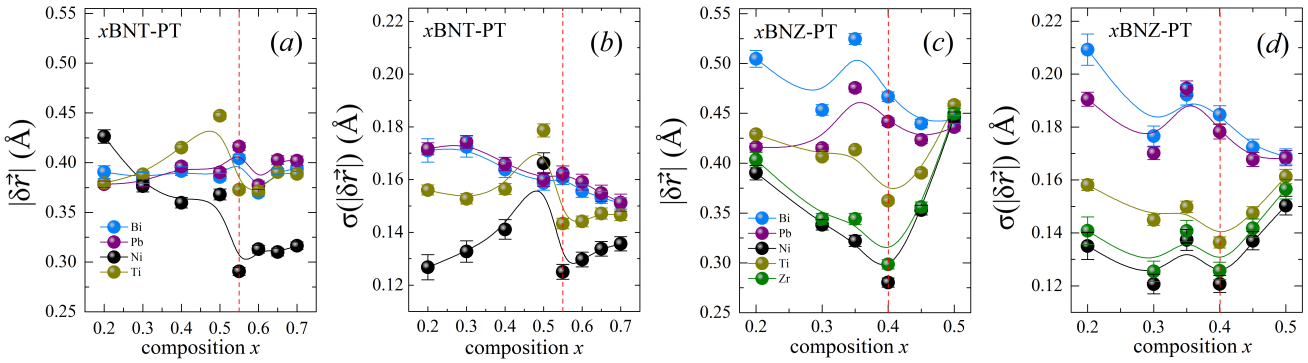

FIG. 4. Mean displacements ($|\delta\vec{r}|_{\text{mean}}$) and their standard deviations [$\sigma(|\delta\vec{r}|)$] as a function of composition for both solid solutions. The histograms of the magnitudes ($|\delta\vec{r}|$) can be found in SM Fig. S7. The histograms of the magnitudes conform to the direction trends as shown in Fig.1 (Fig. S5), meaning that $|\delta\vec{r}|_{\text{mean}}$ can be used as the characteristic parameter of the system. Solid lines in the plots are only guides to eye.

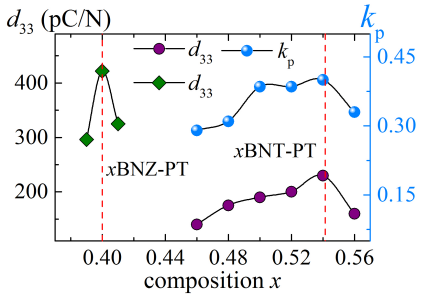

FIG. 5. Reported piezoelectric properties for (*a*) *x*BNT-PT and (*b*) *x*BNZ-PT ceramic samples, taken from References[29] and[18], respectively.

tion to identify the critical point as an MPB in a phase diagram where significant enhancement of the properties can be achieved.

Altogether, it suffices to say that the anomalous enhancement of the piezoelectric properties in *x*BNZ-PT with respect to *x*BNT-PT is an overall effect of the complete flattening of the free energy surfaces for all cations occurring together with the strong dynamic coupling between the A- and B- site cations at the MPB. Naturally these results have general implications in classifying the roles of different atomistic mechanism that drives the properties at an MPB. The current results together with our earlier reports on other ferroelectric solid solutions[17,36] show unequivocally that the softening of the A-BO_3 phonon mode is an indispensable event occurring exactly at the MPB and therefore, strongly suggest that this coupling has a major role in determining the properties. However to maximize the effect of property-enhancement the flattening of the local-potential surfaces is necessary. The exact relative enhancement would also depend on the structural polarity ($|\delta\vec{r}|_{\text{mean}}$), and this is probably why Pb-based systems, where Pb^{2+} seems to maintain a steady and large values of local distortion irrespective of the chemical substitutions,[8] exhibit supe-

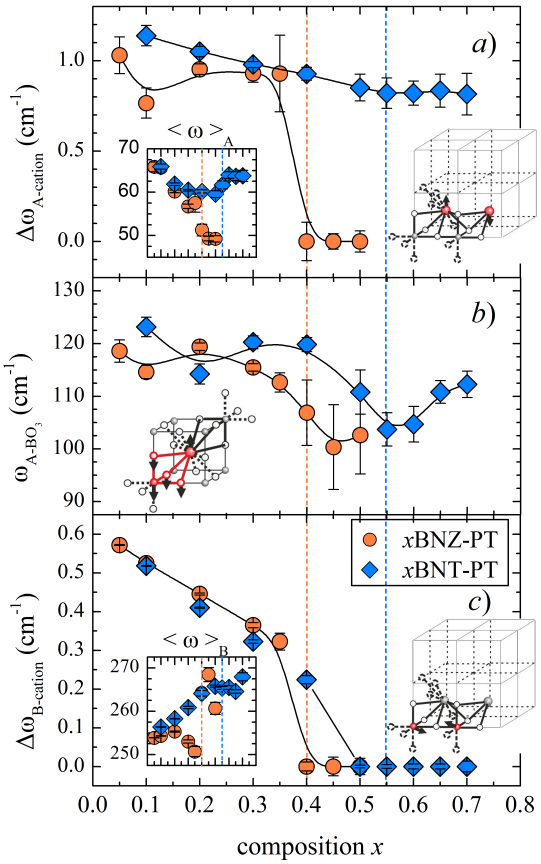

FIG. 6. Development of $\Delta\omega$ and $< \omega >$ parameters comprising discrete vibrations of A-site cations (*a*), B-site cations (*c*), and the phonon mode ω_3 (*b*) involving both A- and B-site cations. The solid lines in the plots are simply guides to eye. The overall Raman spectra as a function of composition for both systems can be found in Fig. S8. The sketches represent the atomic vibrations of corresponding cubic phonon modes.

rior properties than the Pb-free systems including better thermal stability. Inevitably the full or partial absence of any of the mentioned phenomena will not give rise to the maximum increase in the properties.

Generally speaking, our results have unraveled local structural correlations extending up to a few unit cells that are responsible for the MPB properties of ferroelectric solid solutions, which essentially enrich the established concept related to the rotation of the polarization in a strain-reduced environment. We can now say that the mere existence of a low-symmetry phase(s) and/or structural instability facilitating polarization-rotation will not ensure the greatest MPB properties, unless the pivotal alliance occurs between the atomic vibrations and the flattening of the free-energy surfaces for all constituent cations. Besides it is equally important that the system should retain or obtain higher values of inherent structural polarity.

The above atomistic features of a composition-induced phase transition not only expose more fundamental structure-property connections based on static and dynamic information, but more importantly invoke fingerprinting of MPBs where strong amplification of piezoelectric properties can be accomplished. As such, this helps to classify seemingly similar MPBs with varied level of performances and above all provides directions for the improvements. Therefore in terms of either contriving new materials or tweaking the properties, one should consider more of the chemical aspects of the individual elements and their influence on the structure at the mesoscopic-scale instead of the changes in the average structure. We presume that simultaneous substitutions on A and B sites with a *large elastic mismatch* would be helpful to develop essential effects – static and dynamic – in order to bring about the best properties.

ACKNOWLEDGMENTS

Financial support by the Deutsche Forschungsgemeinschaft (MI 1127/8-1) is gratefully acknowledged. The research at ORNL's Spallation Neutron Source was sponsored by the Scientific User Facilities Division, Office of Basic Energy Sciences, U.S. Department of Energy.

* kaustuv.datta@uni-hamburg.de

[1] H. Fu and R. Cohen, Nature **403**, 281 (2000).
[2] B. Noheda, D. E. Cox, G. Shirane, S. E. Park, L. E. Cross, and Z. Zhong, Phys. Rev. Lett. **86**, 3891 (2001).
[3] M. Ahart, M. Somayazulu, R. E. Cohen, P. Ganesh, P. Dera, H. Mao, R. Hemley, Y. Ren, P. Liermann, and Z. Wu, Nature **451**, 545 (2008).
[4] D. Damjanovic, J. Am. Ceram. Soc. **88**, 2663 (2005).
[5] M. Budimir, D. Damjanovic, and N. Setter, Phys. Rev. B **73**, 174106 (2006).
[6] I. Grinberg, V. Cooper, and A. Rappe, Nature **419**, 909 (2002).
[7] I. Grinberg and A. M. Rappe, Phys. Rev. B **70**, 220101(R) (2004).
[8] T. Egami, Annu. Rev. Mater. Res. **37**, 297 (2007).
[9] Y. M. Jin, Y. U. Wang, and a. G. Khachaturyan, Phys. Rev. Lett. **91**, 197601 (2003).
[10] T. Egami, Struct Bond **124**, 69 (2007).
[11] W. Dmowski, S. Vakhrushev, I.-K. Jeong, M. Hehlen, F. Trouw, and T. Egami, Phys. Rev. Lett. **100**, 137602 (2008).
[12] R. G. Burkovsky, Y. A. Bronwald, A. V. Filimonov, A. I. Rudskoya, D. Chernyshov, A. Bosak, J. Hlinka, X. Long, Z.-G. Ye, and S. B. Vakhrushev, Phys. Rev. Lett. **109**, 097603 (2012).
[13] H. Takenaka, I. Grinberg, and A. Rappe, Phys. Rev. Lett. **110**, 147602 (2013).
[14] W. Ge, C. P. Devreugd, D. Phelan, Q. Zhang, M. Ahart, J. Li, H. Luo, L. a. Boatner, D. Viehland, and P. M. Gehring, Phys. Rev. B **88**, 174115 (2013).
[15] N. Zhang, H. Yokota, A. M. Glazer, Z. Ren, D. A. Keen, D. S. Keeble, P. A. Thomas, and Z.-G. Ye, Nat. Commun. **5**, 5231 (2014).
[16] K. Datta, A. Richter, M. Göbbels, D. A. Keen, and R. B. Neder, Phys. Rev. B **93**, 064102 (2016).
[17] K. Datta, R. B. Neder, J. Chen, J. C. Neuefeind, and B. Mihailova, Scientific Reports **7**, 471 (2017).
[18] Y. Rong, J. Chen, H. Kang, L. Liu, L. Fang, L. Fan, Z. Pan, and X. Xing, J. Am. Ceram. Soc. **96**, 1035 (2013).
[19] S. M. Choi, C. J. Stringer, T. R. Shrout, and C. A. Randall, J. Appl. Phys. **98**, 034108 (2005).
[20] R. Eitel, C. Randall, T. Shrout, P. Rehrig, W. Hackenberger, and S.-E. Park, Jpn. J. Appl. Phys. **40**, 5999 (2001).
[21] Z. Pan, J. Chen, L. Fan, L. Liu, L. Fang, and X. Xing, J. Appl. Phys. **112**, 114120 (2012).
[22] Z. Xie, Z. Yue, G. Ruehl, B. Peng, J. Zhang, Q. Yu, X. Zhang, and L. Li, Appl. Phys. Lett. **104**, 243902 (2014).
[23] P. Hu, J. Chen, J. Deng, and X. Xing, J. Am. Chem. Soc. **132**, 1925 (2010).
[24] M. G. Tucker, M. T. Dove, and D. A. Keen, J. Appl. Cryst. **34**, 630 (2001).
[25] R. L. McGreevy, J. Phys. Cond. Matter **13**, 877 (2001).
[26] R. B. Neder and T. Proffen, *Diffuse scattering and defect structure simulations - A cook book using the program DISCUS* (Oxford University Press, UK, 2007).
[27] See Supplemental Material [url] for additional figures and more details on the adopted methodology for the data analyses.
[28] D. S. Keeble, E. R. Barney, D. A. Keen, M. G. Tucker, J. Kreisel, and P. A. Thomas, Adv. Funct. Mater. **23**, 185 (2013).
[29] Q. Zhang, M. Jiang, and Z. Li, J. Electroceram **29**, 179 (2012).
[30] D. D. Khalyavin, A. N. Salak, N. P. Vyshatko, A. B. Lopes, N. M. Olekhnovich, A. V. Pushkarev, I. I. Maroz, and Y. V. Radyush, Chem. Mater. **18**, 5104 (2006).
[31] K. Miura, M. Kubota, M. Azuma, and H. Funakubo, Jpn. J. Appl. Phys. **48**, 09KF05 (2009).
[32] G. Tutuncu, L. Fan, J. Chen, X. Xing, and J. Jones, Appl.

Phys. Lett. **104**, 132907 (2014).
[33] J. Shi, I. Grinberg, X. Wang, and A. M. Rappe, Phys. Rev. B **89**, 2 (2014).
[34] M. Ghita, M. Fornari, D. Singh, and S. Halilov, Phys. Rev. B **72**, 054114 (2005).
[35] A.-M. Welsch, B. J. Maier, B. Mihailova, R. J. Angel, J. Zhao, C. Paulmann, J. M. Engel, M. Gospodinov, V. Marinova, and U. Bismayer, Z. Kristallogr. **226**, 126 (2011).
[36] K. Datta, A. Richter, M. Göbbels, R. B. Neder, and B. Mihailova, Phys. Rev. B **90**, 064112 (2014).
[37] K. Datta, A. Richter, M. Göbbels, R. B. Neder, and B. Mihailova, Phys. Rev. B **92**, 024107 (2015).